

REVIEW ARTICLE

Relic neutrino background from cosmological supernovae

Shin'ichiro Ando[†] and Katsuhiko Sato^{†‡}

[†] Department of Physics, School of Science, The University of Tokyo, 7-3-1 Hongo, Bunkyo-ku, Tokyo 113-0033, Japan

[‡] Research Center for the Early Universe, School of Science, The University of Tokyo, 7-3-1 Hongo, Bunkyo-ku, Tokyo 113-0033, Japan

E-mail: ando@utap.phys.s.u-tokyo.ac.jp, sato@phys.s.u-tokyo.ac.jp

Abstract. Present and future observations of supernova relic neutrinos (SRNs), i.e., a cosmological neutrino background from past core-collapse supernova explosions, potentially give us useful information concerning various fields of astrophysics, cosmology and particle physics. We review recent progress of theoretical and observational studies of SRNs, particularly focusing on the detectability and also on implications for cosmic star formation history and neutrino physics.

Submitted to: *New J. Phys.*

1. Introduction

A core-collapse supernova explosion is one of the most spectacular events in astrophysics, and it attracts a great deal of attention from many physicists and astronomers. It also produces a number of neutrinos and 99% of its gravitational binding energy is transformed to neutrinos; detection of the galactic supernova neutrino burst by ground-based large water Čerenkov detectors, such as Super-Kamiokande (SK) and Sudbury Neutrino Observatory (SNO), would provide valuable information on the nature of neutrinos as well as supernova physics. In addition, because supernova explosions have occurred very commonly in both the past and present universe, tracing the cosmic star formation rate (SFR), they should have emitted a great number of neutrinos, which now make a diffuse background, i.e., supernova relic neutrinos (SRNs). Involved physics in SRN ranges quite widely—from cosmic SFR and supernova physics to neutrino properties as elementary particles. Therefore, detecting SRNs or even setting limits on their flux can give us quite useful and unique implications for various fields of astrophysics, cosmology and particle physics. Detectability of SRNs in various detectors and its implications have been discussed in many theoretical papers [1]–[19] from various points of view, about which we discuss in detail in the following part of the present paper.

Flux estimation requires models of neutrino spectrum emitted from each supernova explosion and cosmic SFR. Furthermore, it is experimentally established that neutrinos mix among different flavours, altering the neutrino spectrum at detectors from the original one after neutrinos propagate inside a supernova envelope; this effect should now be taken into account appropriately. In addition to a flux estimation as precise as possible, a detailed discussion of background events, which hinder the SRN detection, is essential; it has been thoroughly studied by Ando, Sato and Totani [12] and we follow their discussion later in this paper. A stringent observational upper limit on the SRN flux is obtained by the SK group [20] and its value is only a factor of 3–6 larger than several theoretical predictions [8]–[10], [12], already ruling out the theoretical upper limit given by Kaplinghat, Steigman and Walker [11] using conservative models. In order to make the SRN detection more likely, a promising method was proposed by Beacom and Vagins [21]. Their basic idea is to dissolve gadolinium trichloride (GdCl_3) into the water Čerenkov detectors, which greatly reduces the background events if it is applied to the currently working or proposed future detectors such as SK, Hyper-Kamiokande (HK) and Underground Nucleon Decay and Neutrino Observatory (UNO). Therefore, we are now at an exciting stage, where SRNs would soon be detected actually, and be used to obtain several implications for various fields of astrophysics as a unique and complementary method to usual observations of the light.

Since we have a promising prospects of the SRN detection, it is timely to discuss the SRN potential for probing the universe or particle physics. Cosmic SFR is one of such possibilities. The most popular method inferring SFR is to use the galaxy luminosity function of rest-frame ultraviolet (UV) radiation [22]–[30], in addition to far-infrared (FIR)/sub-millimeter dust emission [31, 32] and near-infrared (NIR) $\text{H}\alpha$ line

emission [33]–[36]. In these traditional approaches, however, there are a fair number of ambiguities when the actual observables are converted into the cosmic SFR [37]. The most serious problem is that the effects of dust extinction are non-negligible, especially for rest-frame UV observations. For the approach using SRNs, on the other hand, we are not troubled by such a problem, because neutrinos are completely free of dust extinction. This point is the same with observations in the sub-millimeter wave band; however, neutrinos are emitted directly from stars, whereas sub-millimeter radiation comes from dust and is an indirect process. Another advantage is that supernovae are directly connected with the death of massive stars with $M \gtrsim 8M_\odot$, whose lifetime is expected to be very short compared with the Hubble time-scale H_0^{-1} . It enables direct inference of the cosmic SFR assuming the initial mass function (IMF), not bothered with uncertainty concerning the galaxy luminosity function, which sometimes causes difficulty in the case of rest-frame UV observation [37]. Motivated by all of these reasons, many researchers have investigated the dependence of the SRN flux on various models of cosmic SFR or to what extent the SFR can be probed from the future SRN observations. Totani, Sato and Yoshii [8] gave flux estimation using several theoretical models of galaxy evolution. After the bursting release of the observational SFR data points since the pioneering study by Madau *et al* [23], the SRN flux has been estimated using these SFR results [9, 10, 12]. More recently, theoretical SRN flux calculations have been compared with the observational upper limit by SK [20]. Fukugita and Kawasaki [13] used the limit to obtain constraints on the cosmic SFR; Strigari *et al* [16] adopted the latest SFR model based on the Sloan Digital Sky Survey [38] and concluded that their median SRN flux is slightly below the current SK upper limit. Following the proposal to dissolve Gd into detectors [21], Ando [17] investigated potential performance of the Gd-loaded water Čerenkov detectors such as SK, HK and UNO, using the Monte Carlo (MC) simulation, especially focusing on how reliably an assumed SFR model can be reproduced from the SRN observation.

Neutrino properties can also be probed by the SRN observation in principle. It is pointed out that the resulting SRN signal depends on neutrino oscillation models [14]; particularly if the mass hierarchy is inverted, i.e., the first mass eigenstate that most strongly couples to electron flavour is heavier than the third state, $m_1 > m_3$, and the value of θ_{13} , which has not been well constrained yet, is sufficiently large, then the flavour conversion during propagation inside the supernova envelope could considerably change the neutrino signal. Another interesting possibility is that a stringent constraint can be set on neutrino decay models from the SRN observation as first pointed out by Ando [15] and successively studied by Fogli *et al* [18]. Non-radiative neutrino decay can be induced by the interaction between neutrinos and massless or very light particles such as Majoron. The strongest lower limit to the neutrino lifetime-to-mass ratio is obtained from the solar neutrino observation [39]–[41] and meson decay [42]–[44] to be $\tau/m \gtrsim 10^{-4}$ s/eV. SRN observation, on the other hand, is sensitive to $\sim 10^{10}$ s/eV, which is many orders of magnitude larger than the current limit. This is because of the much longer baseline between the Earth and cosmological supernovae, from which

SRNs are emitted, than 1 AU in the case of solar neutrino observations. Neutrino decay could also change the detected signal from high-energy astrophysical objects [45] or the galactic supernova explosions [46]–[48], and could alter usual discussions on the early universe and structure formation [49] as well as on supernova coolings [50]–[52]; but we stress that in principle we can obtain the most stringent constraints on the neutrino lifetime from the SRN observations.

This paper is organized as follows. We first introduce formulation for calculating the SRN flux in section 2. Models of cosmic SFR, supernova neutrino spectrum calculated by various groups are given in the same section. Neutrino oscillation inside the supernova envelope is briefly described there. SRN flux and event rate at ground-based detectors calculated with our reference models are given in section 3. Section 4 is devoted to a detailed discussion on background events against the SRN detection and detectability at various detectors. Current observational limit by SK, which is obtained by a statistical argument including background events, is briefly summarized also in the same section. We discuss implications of the SRN observation for cosmic SFR and neutrino properties such as oscillation and decay in sections 5 and 6, respectively. Finally, we conclude this paper by giving brief summary in section 7. Throughout this paper, we only consider electron anti-neutrinos ($\bar{\nu}_e$) at detectors because this kind of flavour is most easily detected at the water Čerenkov detectors, on which we mainly focus.

2. Formulation and models

2.1. Formulation

The present number density of SRNs ($\bar{\nu}_e$), whose energy is in the interval $E_\nu \sim E_\nu + dE_\nu$, emitted in the redshift interval $z \sim z + dz$, is given by

$$\begin{aligned} dn_\nu(E_\nu) &= R_{\text{SN}}(z)(1+z)^3 \frac{dt}{dz} dz \frac{dN_\nu(E'_\nu)}{dE'_\nu} dE'_\nu (1+z)^{-3} \\ &= R_{\text{SN}}(z) \frac{dt}{dz} dz \frac{dN_\nu(E'_\nu)}{dE'_\nu} (1+z) dE_\nu, \end{aligned} \quad (1)$$

where $E'_\nu = (1+z)E_\nu$ is the energy of neutrinos at redshift z , which is now observed as E_ν ; $R_{\text{SN}}(z)$ represents the supernova rate per comoving volume at z , and hence the factor $(1+z)^3$ should be multiplied to obtain the rate per physical volume at that time; dN_ν/dE_ν is the number spectrum of neutrinos emitted by one supernova explosion; and the factor $(1+z)^{-3}$ comes from the expansion of the universe. The Friedmann equation gives the relation between t and z as

$$\frac{dz}{dt} = -H_0(1+z)\sqrt{\Omega_m(1+z)^3 + \Omega_\Lambda}, \quad (2)$$

and we adopt the standard Λ CDM cosmology ($\Omega_m = 0.3$, $\Omega_\Lambda = 0.7$, and $H_0 = 70 h_{70} \text{ km s}^{-1} \text{ Mpc}^{-1}$).[§] We now obtain the differential number flux of SRNs, dF_ν/dE_ν ,

[§] Although we use the specific cosmological model here, the SRN flux itself is completely independent of such cosmological parameters, as long as we use observationally inferred SFR models; see their cancellation between equations (3) and (4).

using the relation $dF_\nu/dE_\nu = c dn_\nu/dE_\nu$:

$$\frac{dF_\nu}{dE_\nu} = \frac{c}{H_0} \int_0^{z_{\max}} R_{\text{SN}}(z) \frac{dN_\nu(E'_\nu)}{dE'_\nu} \frac{dz}{\sqrt{\Omega_m(1+z)^3 + \Omega_\Lambda}}, \quad (3)$$

where we assume that gravitational collapses began at the redshift $z_{\max} = 5$.

2.2. Models for cosmic star formation rate

As our reference model for the SFR, we adopt a model that is based on recent progressive results of rest-frame UV, NIR H α , and FIR/sub-millimeter observations; a simple functional form for the SFR per unit comoving volume is given as [53]

$$\psi_*(z) = 0.32 f_* h_{70} \frac{\exp(3.4z)}{\exp(3.8z) + 45} \frac{\sqrt{\Omega_m(1+z)^3 + \Omega_\Lambda}}{(1+z)^{3/2}} M_\odot \text{ yr}^{-1} \text{ Mpc}^{-3}, \quad (4)$$

where f_* is a factor of order unity, which we illustrate below. Figure 1 shows the SFR $\psi_*(z)$ with the various data points from rest-frame UV [22, 23, 30], H α line [33]–[35], and FIR/sub-millimeter [31, 32] observations; these data points are not corrected for dust extinction. In the local universe, all studies show that the comoving SFR monotonically increases with z out to a redshift of at least 1. Although there is such a general observational tendency, even the local ($z = 0$) SFR density is far from precise determination; it ranges fairly widely as $\psi_*(0) = (0.5\text{--}2.9) \times 10^{-2} h_{70} M_\odot \text{ yr}^{-1} \text{ Mpc}^{-3}$ [54]. For this reason, we introduce the correction factor f_* . Our reference model (4) with $f_* = 1$ is consistent with mildly dust-corrected UV data at low redshift; on the other hand, it may underestimate the results of the other wave band observations. In fact, it predicts the local SFR value of $0.7 \times 10^{-2} h_{70} M_\odot \text{ yr}^{-1} \text{ Mpc}^{-3}$, which is close to the lower limit of the estimation by Baldry and Glazebrook [54], but we stress that the SRN flux given below using this model can be simply applied to the other cases if we adjust the correction factor f_* , and would be quite general. Calculations by Strigari *et al* [16] are based on the SFR model giving local value of $1.6 \times 10^{-2} M_\odot \text{ yr}^{-1} \text{ Mpc}^{-3}$, which corresponds to $f_* = 2.3$ in our notation. Although the SFR- z relation generally tends to increase from $z = 0$ to ~ 1 , behaviours at the higher redshift region $z > 1$ are not clear at all. Ando *et al* [12] also investigated the dependence on the several adopted SFR models, which were only different at high-redshift regions ($z \gtrsim 1.5$); our reference model (4) was referred to as the ‘‘SF1’’ model there. They showed that the SRN flux at $E_\nu > 10$ MeV is highly insensitive to the difference among the SFR models (owing to the energy redshift, as discussed in section 3.1).

We obtain the supernova rate ($R_{\text{SN}}(z)$) from the SFR by assuming the Salpeter IMF ($\phi(m) \propto m^{-2.35}$) with a lower cutoff around $0.5M_\odot$, and that all stars with $M > 8M_\odot$ explode as core-collapse supernovae, i.e.,

$$R_{\text{SN}}(z) = \frac{\int_{8M_\odot}^{125M_\odot} dm \phi(m)}{\int_0^{125M_\odot} dm m\phi(m)} \psi_*(z) = 0.0122 M_\odot^{-1} \psi_*(z). \quad (5)$$

Here we assume that the IMF does not change with time, which may be a good approximation provided there are no significant correlations between the IMF and

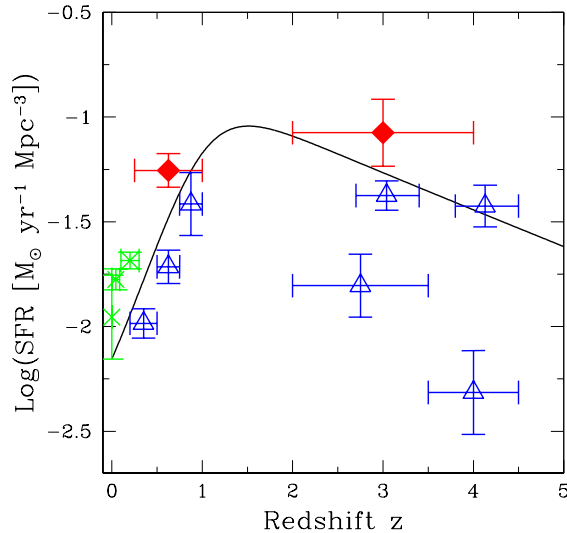


Figure 1. Cosmic star formation rate as a function of redshift. Data points are given by rest-frame UV (*open triangles*) [22, 23, 30], NIR H α (*crosses*) [33, 34, 35], and FIR/sub-millimeter (*filled diamonds*) [31, 32] observations. The solid curve represents our reference model given by equation (4) with $f_* = 1$. The standard Λ CDM cosmology is adopted ($\Omega_m = 0.3, \Omega_\Lambda = 0.7, H_0 = 70 \text{ km s}^{-1} \text{ Mpc}^{-1}$).

the environment in which stars are born; extant evidence seems to argue against such correlations over the redshift range of interest ($z \lesssim 2$) [55]. The resulting local supernova rate evaluated with $f_* = 1$ agrees within errors with the observed value of $R_{\text{SN}}(0) = (1.2 \pm 0.4) \times 10^{-4} h_{70}^3 \text{ yr}^{-1} \text{ Mpc}^{-3}$ (e.g., [56] and references therein). In fact, the totally time-integrated neutrino spectrum from massive stars ($\gtrsim 30 M_\odot$) could be very different from the models that we use (and give in the next subsection), possibly because of, e.g., black hole formation. However, the conversion factor appearing in equation (5) is highly insensitive to the upper limit of the integral in the numerator; for instance, if we change the upper limit in the numerator to $25 M_\odot$, the factor becomes $0.010 M_\odot^{-1}$, which is only slightly different from the value in equation (5).

2.3. Neutrino spectrum from supernova explosions

For the neutrino spectrum from each supernova, we adopt three reference models by different groups, i.e., simulations by the Lawrence Livermore (LL) group [57] and Thompson, Burrows and Pinto [58] (hereafter TBP), and the MC study of spectral formation by Keil, Raffelt and Janka [59] (hereafter KRJ). In this field, however, the most serious problem is that the recent sophisticated hydrodynamic simulations have not obtained the supernova explosion itself; the shock wave cannot penetrate the entire core. Therefore, many points still remain controversial, e.g., the average energy ratio among neutrinos of different flavours, or how the gravitational binding energy is distributed to each flavour. All these problems are quite serious for our estimation, since the binding

Table 1. Fitting parameters for supernova neutrino spectrum.

Model	Mass (M_\odot)	$\bar{E}_{\bar{\nu}_e}$ (MeV)	\bar{E}_{ν_x} (MeV)	$\beta_{\bar{\nu}_e}$	β_{ν_x}	$L_{\bar{\nu}_e}$ (erg)	L_{ν_x} (erg)
LL [57]	20	15.4	21.6	3.8	1.8	4.9×10^{52}	5.0×10^{52}
TBP [58]	11	11.4	14.1	3.7	2.2	—	—
	15	11.4	14.1	3.7	2.2	—	—
	20	11.9	14.4	3.6	2.2	—	—
KRJ [59]	—	15.4	15.7	4.2	2.5	—	—

energy released as $\bar{\nu}_e$ changes the normalization of the SRN flux, and the average energy affects the SRN spectral shape. Traditionally, neutrino spectrum is assumed to have a Fermi-Dirac spectral shape with $T_{\bar{\nu}_e} \simeq 5$ MeV and $T_{\nu_x} \simeq 8$ MeV, where ν_x represents non-electron neutrinos and anti-neutrinos, as adopted in many studies including recent ones [7]–[11], [13, 16, 19]. This approximation is roughly consistent with the LL model, although slight difference exists at both high- and low-energy regions [12, 57]. The other two models (TBP and KRJ) that are more sophisticated, however, are not consistent with such simple treatment at all as we describe below or as already discussed in [17]. Because of all these reasons stated above, we believe that these three models from different groups will be complementary.

The numerical simulation by the LL group [57] is considered to be the most appropriate for our estimation, because it is the only model that succeeded in obtaining a robust explosion and in calculating the neutrino spectrum during the entire burst (~ 15 s). According to their calculation, the average energy difference between $\bar{\nu}_e$ and ν_x was rather large and the complete equipartition of the binding energy was realized $L_{\nu_e} = L_{\bar{\nu}_e} = L_{\nu_x}$, where L_{ν_α} represents the released gravitational energy as α -flavour neutrinos. The neutrino spectrum obtained by their simulation is well fitted by a simple formula, which was originally given by KRJ as

$$\frac{dN_\nu}{dE_\nu} = \frac{(1 + \beta_\nu)^{1+\beta_\nu} L_\nu}{\Gamma(1 + \beta_\nu) \bar{E}_\nu^2} \left(\frac{E_\nu}{\bar{E}_\nu} \right)^{\beta_\nu} e^{-(1+\beta_\nu)E_\nu/\bar{E}_\nu}, \quad (6)$$

where \bar{E}_ν is the average energy; the values of the fitting parameters for the $\bar{\nu}_e$ and ν_x spectrum are summarized in Table 1.

Although the LL group succeeded in obtaining a robust explosion, their result has recently been criticized because it lacked many relevant neutrino processes that are now recognized as important. Thus, we adopt the recent result of another hydrodynamic simulation, the TBP one, which included all the relevant neutrino processes, such as neutrino bremsstrahlung and neutrino-nucleon scattering with nucleon recoil. Their calculation obtained no explosion, and the neutrino spectrum ends at 0.25 s after core bounce. In the strict sense, we cannot use their result as our reference model because the fully time-integrated neutrino spectrum is definitely necessary in our estimate. However, we adopt their result in order to confirm the effects of recent sophisticated treatments of neutrino processes in the supernova core on the SRN spectrum. The TBP calculations

include three progenitor mass models, i.e., 11, 15 and $20M_{\odot}$; all of these models are well fitted by equation (6), and the fitting parameters are summarized in table 1. The average energy for both $\bar{\nu}_e$ and ν_x is much smaller than that by the LL calculation. Although we do not show this in table 1, it was also found that at least for the early phase of the core-collapse, the complete equipartition of the gravitational binding energy for each flavour was not realized. However, it is quite unknown whether these trends hold during the entire burst. In this study, we adopt the average energy given in table 1 as our reference model, while we assume perfect equipartition between flavours, i.e., $L_{\bar{\nu}_e} = L_{\nu_x} = 5.0 \times 10^{52}$ erg.

In addition, we also use the model by KRJ. Their calculation did not couple with the hydrodynamics, but it focused on the spectral formation of neutrinos of each flavour using an MC simulation. Therefore, the static model was assumed as a background of neutrino radiation, and we use their “accretion phase model II,” in which the neutrino transfer was solved in the background of a 150 ms postbounce model by way of a general relativistic simulation. The fitting parameters for their MC simulation are also summarized in table 1. Unlike the previous two calculations, their result clearly shows that the average energy of ν_x is very close to that of $\bar{\nu}_e$. It also indicates that the equipartition among each flavour was not realized, but rather $L_{\nu_e} \simeq L_{\bar{\nu}_e} \simeq 2L_{\nu_x}$. However also in this case, since the totally time-integrated neutrino flux is unknown from such temporary information, we assume perfect equipartition, $L_{\bar{\nu}_e} = L_{\nu_x} = 5.0 \times 10^{52}$ erg, as well as that the average energies are the same as those in table 1.

2.4. Neutrino spectrum after neutrino oscillation

The original $\bar{\nu}_e$ spectrum is different from what we observe as $\bar{\nu}_e$ at Earth, owing to the effect of neutrino oscillation. Since the specific flavour neutrinos are not mass eigenstates, they mix with other flavour neutrinos during their propagation. The behaviour of flavour conversion inside the supernova envelope is well understood, because the relevant mixing angles and mass square differences are fairly well determined by recent solar [60, 61], atmospheric [62], and reactor neutrino experiments [63]. The remaining ambiguities concerning the neutrino oscillation parameters are the value of θ_{13} , which is only weakly constrained ($\sin^2 \theta_{13} \lesssim 0.1$ [64]), and the type of mass hierarchy, i.e., normal ($m_1 \ll m_3$) or inverted ($m_1 \gg m_3$). We first discuss the case of normal mass hierarchy as our standard model; in this case, the value of θ_{13} is irrelevant. The case of inverted mass hierarchy is addressed in section 6.1. In addition, other exotic mechanisms, such as resonant spin-flavour conversion (see [65] and references therein) and neutrino decay [15, 18], which possibly change the SRN flux and spectrum, might work in reality, and these topics are also discussed later in sections 6.2 and 6.3, respectively.

The produced $\bar{\nu}_e$ at the supernova core are coincident with the lightest mass eigenstate $\bar{\nu}_1$ owing to the large matter potentials. Since this state $\bar{\nu}_1$ is the lightest also in vacuum, there are no resonance regions in which one mass eigenstate can change

into another state, and therefore $\bar{\nu}_e$ at production arrives at the stellar surface as $\bar{\nu}_1$. Thus, the $\bar{\nu}_e$ spectrum observed by the distant detector is

$$\begin{aligned} \frac{dN_{\bar{\nu}_e}}{dE_{\bar{\nu}_e}} &= |U_{e1}|^2 \frac{dN_{\bar{\nu}_1}}{dE_{\bar{\nu}_1}} + |U_{e2}|^2 \frac{dN_{\bar{\nu}_2}}{dE_{\bar{\nu}_2}} + |U_{e3}|^2 \frac{dN_{\bar{\nu}_3}}{dE_{\bar{\nu}_3}} \\ &= |U_{e1}|^2 \frac{dN_{\bar{\nu}_e}^0}{dE_{\bar{\nu}_e}} + (1 - |U_{e1}|^2) \frac{dN_{\nu_x}^0}{dE_{\nu_x}}, \end{aligned} \quad (7)$$

where the quantities with superscript 0 represent those at production, $U_{\alpha i}$ is the mixing matrix element between the α -flavour state and i -th mass eigenstate, and observationally $|U_{e1}|^2 = 0.7$. In other words, 70% of the original $\bar{\nu}_e$ survives; on the other hand, the remaining 30% comes from the other component ν_x . Therefore, both the original $\bar{\nu}_e$ and ν_x spectra are necessary for the estimation of the SRN flux and spectrum; since the original ν_x spectrum is generally harder than that of the original $\bar{\nu}_e$, as shown in table 1, the flavour mixing is expected to harden the detected SRN spectrum.

3. Flux and event rate of supernova relic neutrinos

3.1. Flux of supernova relic neutrinos

The SRN flux can be calculated by equation (3) with our reference models given in section 2. Figure 2(a) shows the SRN flux as a function of neutrino energy for the three supernova models, LL, TBP and KRJ. The flux of atmospheric $\bar{\nu}_e$, which becomes background events for SRN detection, is shown in the same figure [66, 67]. The SRN flux peaks at $\lesssim 5$ MeV, and around this peak, the TBP model gives the largest SRN flux because the average energy of the original $\bar{\nu}_e$ is considerably smaller than in the other two models but the total released energy is assumed to be the same. On the other hand, the model gives a smaller contribution at high-energy regions, $E_\nu > 10$ MeV. In contrast, the high-energy tail of the SRN flux with the LL model extends farther than with the other models, and it gives flux more than a order of magnitude larger at $E_\nu = 60$ MeV. This is because the high-energy tail was mainly contributed by the harder component of the original neutrino spectrum; in the case of the LL calculation, the average energy of the harder component ν_x is significantly larger than that of the other two calculations, as shown in table 1. We show the values of the SRN flux integrated over the various energy ranges in table 2. The total flux is expected to be 11–16 $f_* \text{ cm}^{-2} \text{ s}^{-1}$ for our reference models, although this value is quite sensitive to the shape of the assumed SFR, especially at high- z . The energy range in which we are more interested is high-energy regions such as $E_\nu > 19.3$ MeV and $E_\nu > 11.3$ MeV, because as discussed below, the background events are less critical and the reaction cross section increases as $\propto E_\nu^2$. In such a range, the SRN flux is found to be 1.3–2.3 $f_* \text{ cm}^{-2} \text{ s}^{-1}$ ($E_\nu > 11.3$ MeV) and 0.14–0.46 $f_* \text{ cm}^{-2} \text{ s}^{-1}$ ($E_\nu > 19.3$ MeV). Thus, the uncertainty about the supernova neutrino spectrum and its luminosity gives at least a factor 2–4 ambiguity to the expected SRN flux in the energy region of our interest.

Figure 2(b) shows the contribution by supernova neutrinos emitted from various

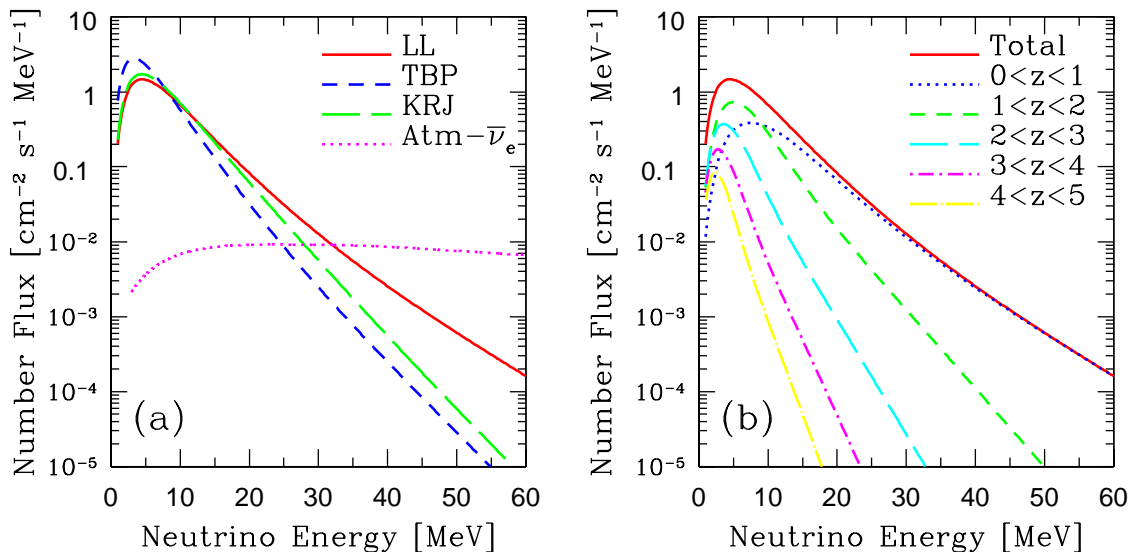


Figure 2. (a) SRN flux in units of $f_* \text{ cm}^{-2} \text{ s}^{-1} \text{ MeV}^{-1}$ calculated with three reference models of original neutrino spectrum: LL, TBP and KRJ. The flux of atmospheric neutrinos [66, 67] is also shown for comparison. (b) The same as (a), but indicating contribution from various redshift ranges. LL is adopted as the supernova model. These figures are taken from [17].

Table 2. Flux of supernova relic neutrinos.

Model	Redshift range	Flux ($f_* \text{ cm}^{-2} \text{ s}^{-1}$)		
		Total	$E_\nu > 11.3 \text{ MeV}$	$E_\nu > 19.3 \text{ MeV}$
LL	Total	11.7	2.3	0.46
	$0 < z < 1^a$	4.1 (35.3)	1.6 (70.9)	0.39 (85.2)
	$1 < z < 2^a$	4.9 (42.0)	0.6 (26.3)	0.06 (14.0)
	$2 < z < 3^a$	1.8 (15.1)	0.1 (2.5)	0.0 (0.7)
	$3 < z < 4^a$	0.6 (5.3)	0.0 (0.2)	0.0 (0.0)
	$4 < z < 5^a$	0.2 (2.1)	0.0 (0.0)	0.0 (0.0)
TBP	Total	16.1	1.3	0.14
KRJ	Total	12.7	2.0	0.28

^a Contribution from each redshift range to the total ($0 < z < 5$) value are shown in parentheses as percentages.

redshift ranges. At high-energy region $E_\nu > 10 \text{ MeV}$, the dominant flux comes from the local supernovae ($0 < z < 1$), while the low-energy side is mainly contributed by the high-redshift events ($z > 1$). This is because the energy of neutrinos that were emitted from a supernova at redshift z is reduced by a factor of $(1+z)^{-1}$ reflecting the expansion of the universe, and therefore high-redshift supernovae only contribute to low-energy flux. We also show the energy-integrated flux from each redshift range in table 2 in the case of the LL supernova model. From the table, it is found that in the energy range of our interest, more than 70% of the flux comes from local supernova

explosions at $z < 1$, while the high-redshift ($z > 2$) supernova contribution is very small.

3.2. Event rate at water Čerenkov detectors

The water Čerenkov neutrino detectors have greatly succeeded in probing the properties of neutrinos as elementary particles, such as neutrino oscillation. The SK detector is one of these detectors, and its large fiducial volume (22.5 kton) might enable us to detect the diffuse background of SRNs. Furthermore, much larger water Čerenkov detectors such as HK and UNO are being planned. SRN detection is most likely with the inverse β -decay reaction with protons in water, $\bar{\nu}_e p \rightarrow e^+ n$, and its cross section is precisely understood [68, 69]. In our calculation, we use the trigger threshold of SK-I (before the accident).

The expected event rates at such detectors are shown in figures 3(a) and 3(b) in units of f_* (22.5 kton yr) $^{-1}$ MeV $^{-1}$; with SK, it takes a year to obtain the shown SRN spectrum, while with HK and UNO, much less time [$1 \text{ yr} \times (22.5 \text{ kton}/V_{\text{fid}})$, where V_{fid} is the fiducial volume of HK or UNO] is necessary because of their larger fiducial volume. Figure 3(a) compares the three models of the original supernova neutrino spectrum, and figure 3(b) shows the contribution to the total event rate from each redshift range. In table 3 we summarize the event rate integrated over various energy ranges for three supernova models. The expected event rate is 0.97–2.3 f_* (22.5 kton yr) $^{-1}$ for $E_e > 10$ MeV and 0.25–1.0 f_* (22.5 kton yr) $^{-1}$ for $E_e > 18$ MeV. This clearly indicates that if the background events that hinder the detection are negligible, the SK has already reached the required sensitivity for detecting SRNs; with the future HK and UNO, a statistically significant discussion would be possible. This also shows that the current shortage of our knowledge concerning the original supernova neutrino spectrum and luminosity gives at least a factor of 2 ($E_\nu > 10$ MeV) to 4 ($E_\nu > 18$ MeV) uncertainty to the event rate at the high-energy range (actual detection range). We also summarize the contribution from each redshift range in the same table, especially for the calculation with the LL model. The bulk of the detected events will come from the local universe ($z < 1$), but the considerable flux is potentially attributed to the range $1 < z < 2$.

4. Detectability and observational upper limit

4.1. Background events against detection

In the previous section, we calculated the expected SRN spectrum at the water Čerenkov detectors on the Earth, but the actual detection is quite restricted because of the presence of other background events. In this paper, we follow a detailed consideration of these backgrounds by Ando *et al* [12]. There are atmospheric and solar neutrinos, antineutrinos from nuclear reactors, spallation products induced by cosmic-ray muons and decay products of invisible muons. We show in figures 4(a) and 4(b) the flux and event rate of SRNs and these background events.

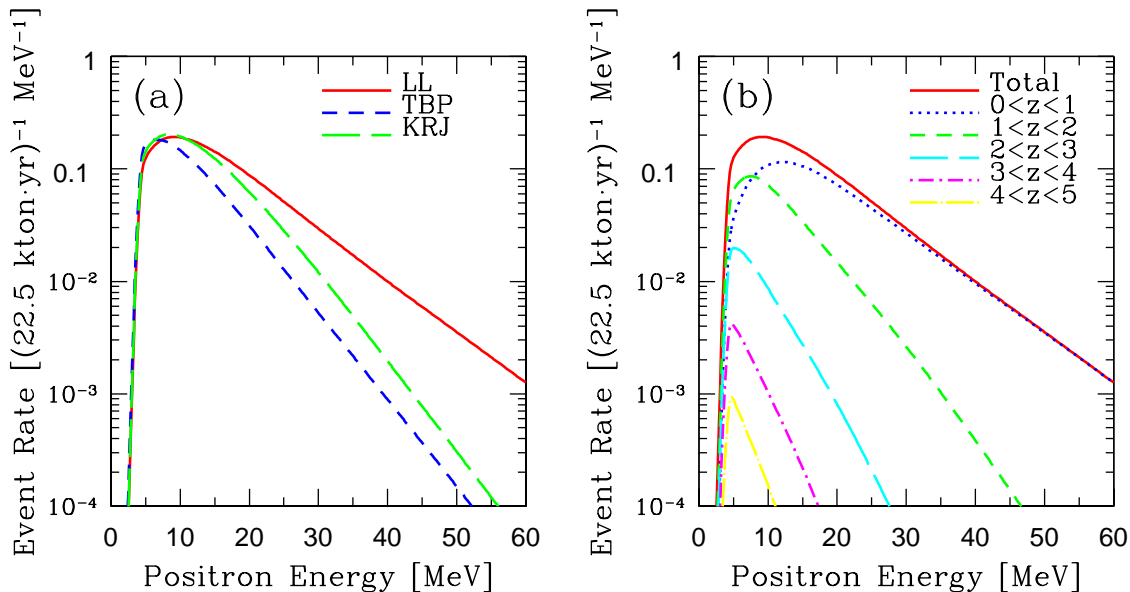


Figure 3. (a) Event rate at water Čerenkov detectors in units of f_* $(22.5 \text{ kton yr})^{-1} \text{ MeV}^{-1}$ for three supernova models. (b) The same as (a), but indicating contribution from various redshift ranges. LL is adopted as the supernova model. These figures are taken from [17].

Table 3. Event rate of supernova relic neutrinos.

Model	Redshift range	Event rate [f_* $(22.5 \text{ kton yr})^{-1}$]	
		$E_e > 10 \text{ MeV}$	$E_e > 18 \text{ MeV}$
LL	Total	2.3	1.0
	$0 < z < 1^a$	1.7 (77.5)	0.9 (87.5)
	$1 < z < 2^a$	0.5 (20.6)	0.1 (11.9)
	$2 < z < 3^a$	0.0 (1.7)	0.0 (0.5)
	$3 < z < 4^a$	0.0 (0.1)	0.0 (0.0)
	$4 < z < 5^a$	0.0 (0.0)	0.0 (0.0)
TBP	Total	0.97	0.25
KRJ	Total	1.7	0.53

^a Contribution from each redshift range to the total ($0 < z < 5$) value are shown in parentheses as percentages.

The flux of the atmospheric neutrinos is usually calculated using MC method including various relevant effects (flux of primary cosmic rays, solar modulation, geomagnetic field, interaction of cosmic rays in the air, and so on), and in that simulation one-dimensional approximation is used, i.e., after the interaction of primary cosmic ray particles with air nuclei, all the particles are assumed to be moving along the line of the momentum vector of the primary cosmic ray particles [70]. (Preliminary results of three-dimensional flux calculations have been reported [71].) There are many authors who calculated the atmospheric neutrino flux (see, e.g., [72]–[74] for recent results). We

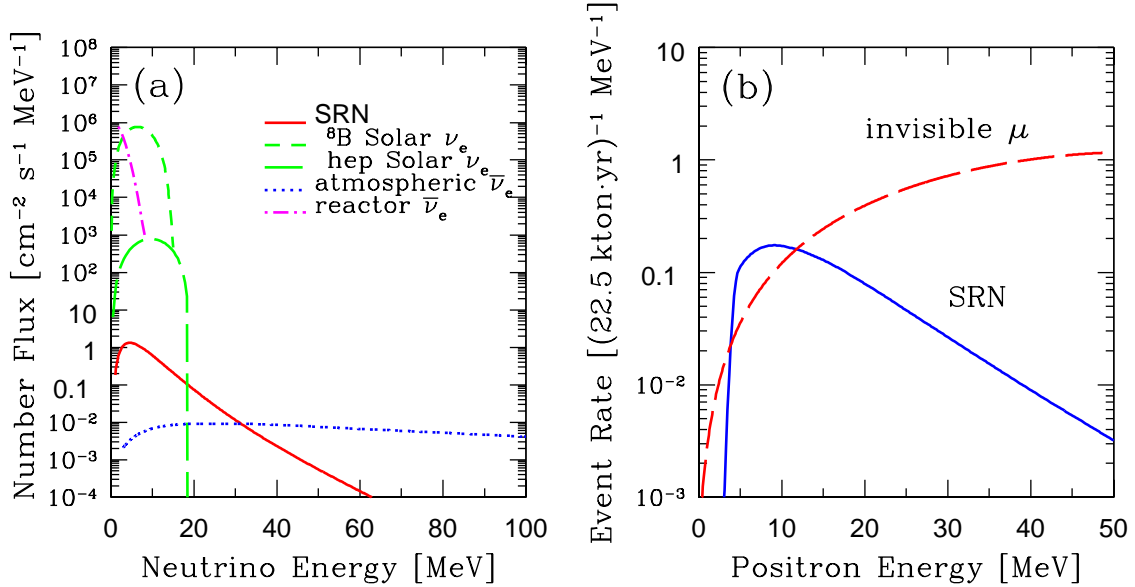


Figure 4. (a) Number flux of SRNs compared with other background neutrinos. (b) Event rate of SRNs and invisible muon decay products. In both panels, LL is adopted as the original neutrino spectrum. These figures are taken from [12].

use in this paper the flux calculated by Gaisser *et al* [66, 67].

Solar neutrino flux is dominant at energy range below 19 MeV. We use the flux predicted by the standard solar model (SSM) in figure 4 [75]. Since the solar neutrinos are not $\bar{\nu}_e$ but ν_e , the cross section for them is about two orders of magnitude smaller than that for $\bar{\nu}_e$. Furthermore recoil electrons scattered by solar neutrinos strongly concentrate to the opposite direction of the Sun, in contrast to the isotropic distribution of $\bar{\nu}_e$ events. Therefore, the solar neutrinos are an avoidable background, not as critical as other events. At the same energy range corresponding to $E_\nu \lesssim 19$ MeV, there is another serious background that becomes an obstacle also for solar neutrino detection, i.e., spallation products induced by cosmic ray muons. The event rate of the spallation background is several hundred per day per 22.5 kton, and it is extremely difficult to reject all of these events. Therefore the solar neutrino range ($E_\nu \lesssim 19$ MeV), cannot be used as an energy window.

The third background which we must consider is anti-neutrinos from nuclear reactors. In each nuclear reactor, almost all the power comes from the fissions of the four isotopes, ²³⁵U (~ 75%), ²³⁸U (~ 7%), ²³⁹Pu (~ 15%) and ²⁴¹Pu (~ 3%) [76]. Each isotope produces a unique electron anti-neutrino spectrum through the decay of its fission fragments and their daughters. The $\bar{\nu}_e$ spectrum from ²³⁵U, ²³⁹Pu and ²⁴¹Pu can be derived using the semi-empirical formula with which we fit data of detected β -spectrum from fission by thermal neutrons [77, 78]. (²³⁸U undergoes only fast neutron fission and hence electron spectrum from ²³⁸U cannot be measured by this kind of experiment.) Above 7 MeV, the number of β counts drops dramatically and fitting

error becomes large. In addition, with this method, as we determine the maximum β energy and derives the energy distribution below that energy, it is difficult to estimate the errors at the high-energy range. While the $\bar{\nu}_e$ spectra in [77, 78] are given as tables, we use for simplicity somewhat less accurate analytical approximation given in [79]. As a normalization factor we use energy-integrated $\bar{\nu}_e$ flux at Kamioka, $1.34 \times 10^6 \text{ cm}^{-2} \text{ s}^{-1}$, which are the summation of the flux from various nuclear reactors in Japan and Korea [76].

With these backgrounds we discussed above and from figure 4(a), we expect the energy window of SRN events ranging 19–30 MeV. However, electrons or positrons from invisible muons are the largest background in the energy window from 19 to 60 MeV. This invisible muon event is illustrated as follows. Atmospheric neutrinos produce muons by interaction with the nucleons (both free and bound) in the fiducial volume. If these muons are produced with energies below Čerenkov radiation threshold (kinetic energy less than 53 MeV), then they will not be detected (“invisible muons”), but successively produced electrons and positrons from the muon decay will be visible. Since this muon decay signal will mimic the $\bar{\nu}_e p \rightarrow e^+ n$ process in SK, it is difficult to distinguish SRN from these events. The spectrum of this invisible muon events is shown in figure 4(b), compared with the SRN spectrum. Therefore, even at the remaining candidate of the energy window 19–30 MeV, there is a huge background due to the invisible muons, resulting in *no energy window* for the SRN detection at present.

4.2. Detectability at pure-water Čerenkov detectors

We expect that SRNs can be most likely detected at water Čerenkov detectors such as SK, because the largest class of volume can be realized, enabling the most statistically significant discussions. The most serious problem is that there is no energy window as we described in the previous subsection. In the energy range 19–30 MeV, the SRN event number is estimated to be $N_{\text{SRN}} = 0.73 f_* (V_{\text{eff}}/22.5 \text{ kton} \cdot \text{yr})$ for the LL model, where we define the effective volume of detectors V_{eff} by (fiducial volume) \times (time) \times (efficiency), which is the relevant quantity representing the detector performance. On the other hand, the background level would be as large as $N_{\text{bg}} \sim 3.4 (V_{\text{eff}}/22.5 \text{ kton} \cdot \text{yr})$, mainly contributed by the invisible muon decay products. Therefore, signal-to-noise ratio S/N can be written as

$$S/N \equiv \frac{N_{\text{SRN}}}{\sqrt{N_{\text{SRN}} + N_{\text{bg}}}} = \frac{0.73 f_*}{\sqrt{0.73 f_* + 3.4}} \left(\frac{V_{\text{eff}}}{22.5 \text{ kton yr}} \right)^{1/2}, \quad (8)$$

plotted in figure 5 as a function of f_* for several values of effective volume. For detectors with the size of SK, one-year observation is found to be insufficient to obtain significant SRN detection. Further data-taking for about 10 years may reach $S/N \lesssim$ a few, but this number is still insufficient in statistical significance. Future mega-ton class detectors such as HK and UNO now planned potentially give us a considerable number of SRN detection, by data-taking for a couple of years, as can be seen from the upper curve in figure 5.

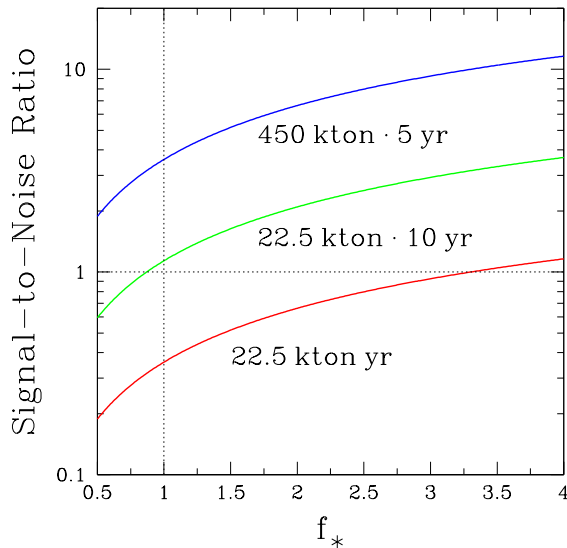


Figure 5. Signal-to-noise ratio S/N of SRNs at pure-water Čerenkov detectors (8), as a function of a correction factor f_* for the SFR model (4). LL is assumed for the original neutrino spectrum. Each line is labeled by the value of the effective volume V_{eff} .

4.3. Detectability at other detectors

In this subsection, we discuss the SRN detectability at SNO (the heavy water Čerenkov detector) and KamLAND (the scintillation detector), which is mainly discussed in [12] and [12, 16], respectively. An advantage of these detectors is that we are able to identify $\bar{\nu}_e$ events using delayed coincidence signals; neutrons produced via $\bar{\nu}_e d \rightarrow e^+ n n$ (SNO) and $\bar{\nu}_e p \rightarrow e^+ n$ (KamLAND) are tagged by deuterons, Cl or He (SNO) and by protons (KamLAND), resulting in γ -ray cascades, identified with the preceded positron signal. Using this technique, we can remove other backgrounds from non- $\bar{\nu}_e$ origin (solar neutrinos, invisible muons and spallation products), opening up an energy window in the range of 10–30 MeV. Unfortunately, because the detector volume is small (both detectors are about 1 kton), the expected SRN rate is quite small, $0.03f_* \text{ yr}^{-1}$ for SNO and $0.1f_* \text{ yr}^{-1}$ for KamLAND [12]. More recently, Strigari *et al* [16] estimated the event rate at KamLAND to be $\sim 0.4 \text{ yr}^{-1}$, but they used the energy range above 6 MeV, simply because there have been no events seen above this energy at KamLAND [63]. In addition, the detectability at liquid argon detectors has been discussed in [19]; although the detection is still challenging, potential advantage is that these detectors can mainly capture ν_e , which is difficult with other detectors.

4.4. Current observational limit and future prospects

The most stringent upper limit on the SRN flux is obtained by the observation for 1496 days (4.1 yr) at the SK detectors [20]. This limit is obtained by the statistical analysis

including the background events from atmospheric neutrinos and invisible muons, and is $< 1.2 \text{ cm}^{-2} \text{ s}^{-1}$ over the energy region of $E_\nu > 19.3 \text{ MeV}$ (90% CL). Comparing with the prediction for the same energy range given in table 2, we find that the current SK limit is only about a factor 2.5–8.5 larger than our prediction using the reference model for the cosmic SFR with $f_* = 1$, depending on the adopted original neutrino spectrum. This strong constraint motivated many theoretical studies [13]–[16] and has been translated into constraints on various quantities as we further discuss in the following sections.

Although the SK limit was derived by a careful analysis of the spectral data over the energy range $E_e > 18 \text{ MeV}$, we here show that a very rough statistical argument using equation (8) can fairly well reproduce the same limit. In equation (8), we consider setting a limit at 90% CL, which corresponds to 1.64σ level (or $S/N < 1.64$), as a result of no SRN detection for $V_{\text{eff}} = 22.5 \text{ kton} \cdot 4.1 \text{ yr}$ observation. Substituting these values into equation (8), it is solved for f_* , resulting in the upper limit $f_* < 2.6$ (90% CL). This value is then translated into the flux limit using the relation between the SRN flux and f_* (for the LL model) given in table 2, i.e., $F_\nu < 1.2 \text{ cm}^{-2} \text{ s}^{-1}$ for $E_\nu > 19.3 \text{ MeV}$ (90% CL), which is in remarkable agreement with the actual result reported by the SK group [20].

In the near future, sensitivity of water Čerenkov detectors for the SRN detection would be significantly improved by the promising technique proposed recently [21]. The basic idea is the same as the delayed coincidence technique actually adopted by SNO or KamLAND (see discussions in section 4.3), but GdCl_3 is dissolved into the pure-water of SK (or other future detectors), which enables us to actively identify $\bar{\nu}_e$ by capturing neutrons produced by the $\bar{\nu}_e p \rightarrow e^+ n$ reaction. Owing to this proposal, the range 10–30 MeV would be an energy window because we can positively distinguish the $\bar{\nu}_e$ signal from other backgrounds such as solar neutrinos (ν_e), invisible muon events and spallation products. The neutron capture efficiency by Gd is estimated to be 90% with the proposed 0.2% admixture by mass of GdCl_3 in water, and subsequently 8 MeV γ -cascade occurs from the excited Gd. The single-electron energy equivalent to this cascade was found to be 3–8 MeV by a careful simulation [80], and with the trigger threshold adopted in SK-I, only about 50% of such cascades can be detected actually. However, it is expected that SK-III, which will begin operation in mid-2006, will trigger at 100% efficiency above 3 MeV, with good trigger efficiency down to 2.5 MeV [21]. In that case most of the γ -cascades from Gd will be detected with their preceding signal of positrons. From this point on, we assume 100% efficiency; even if we abandon this assumption, it does not affect our physical conclusion, since the relevant quantity representing the detector performance is the effective volume V_{eff} that already includes efficiency.

Table 4. Constraints on supernova rate and star formation rate models. Upper part shows the SK limit on the SRN observation [20], whereas lower part shows the results of local supernova surveys [56] and observational inference of the local SFR [54].

	f_*	$R_{\text{SN}}(0)$ ($\text{yr}^{-1} \text{Mpc}^{-3}$)	$\psi_*(0)$ ($M_{\odot} \text{yr}^{-1} \text{Mpc}^{-3}$)
LL	< 2.6	$< 2.2 \times 10^{-4}$	$< 1.8 \times 10^{-2}$
TBP	< 8.6	$< 7.3 \times 10^{-4}$	$< 6.0 \times 10^{-2}$
KRJ	< 4.3	$< 3.6 \times 10^{-4}$	$< 3.0 \times 10^{-2}$
[56]	0.9–1.9	$(0.8\text{--}1.6) \times 10^{-4}$	—
[54]	0.7–4.2	—	$(0.5\text{--}2.9) \times 10^{-2}$

5. Implication for cosmic star formation history

5.1. Constraints from the current observational limit

The current SK upper limit on the SRN flux is already stringent to give some physical or astronomical consequences. In this subsection, we discuss a constraint on the cosmic SFR from the SRN limit; similar arguments have been given in [13]. Comparing with our flux predictions using several supernova models (table 2), the SK limit can be directly translated into the bound on the correction parameter f_* to the cosmic SFR introduced in (4), since the redshift dependence is roughly consistent among various observations. Further, the constraint on f_* can then be used as that on the local supernova rate and SFR. The results are summarized in table 4 for various supernova models. For comparison, in the lower part of the same table, we also show the result of local supernova surveys, $R_{\text{SN}}(0) = (0.8\text{--}1.6) \times 10^{-4} \text{ yr}^{-1} \text{ Mpc}^{-3}$ [56], and the observationally inferred SFR $\psi_*(0) = (0.5\text{--}2.9) \times 10^{-2} M_{\odot} \text{ yr}^{-1} \text{ Mpc}^{-3}$ [54]. In particular for the local SFR, the SK limit on the SRN flux may rule out some fraction of the observationally inferred value, if we choose the LL model for the original neutrino spectrum; for the other two supernova models, the SK limit is very close to the current upper bound on the cosmic SFR by observations with the light. Therefore, we stress that the neutrino observation has already reached sensitivity to the cosmic SFR comparable with the usual and traditional approaches using the light.

5.2. Performance of Gd-loaded detectors

Performance of the proposed Gd-loaded detectors as an SFR probe is of our interest, and has recently been investigated in detail by Ando [17] using the MC simulation; in this subsection, we briefly introduce his discussion. Although we focus here on how far the SFR can be probed by SRN observation, the uncertainty from the supernova neutrino spectrum would give a fair amount of error. However, this problem can be solved if a supernova explosion occurs in our galaxy; the expected event number is about 5000–10,000 at SK, when supernova neutrino burst occurs at 10 kpc, and it will enable a statistically significant discussion concerning the neutrino spectrum from

supernova explosions. Even if there are no galactic supernovae in the near future, remarkable development of the supernova simulation can be expected with the growth of computational resources and numerical technique. With such developments, the supernova neutrino spectrum and luminosity may be uncovered, and the ambiguity is expected to be reduced significantly. Thus, in this paper we assume that the supernova neutrino spectrum is well understood and that our reference models are fairly good representatives of nature; we analyze the SFR alone with several free parameters.

The basic procedure adopted in [17] is as follows. (1) The expected signal (spectrum) at a Gd-loaded detector in the range 10–30 MeV is simulated, assuming that there are no background events. In that process, the SFR given by equation (4) with $f_* = 1$ and the LL model as neutrino spectrum are used for the generation of the SRN signal. (2) Then the SRN spectrum is analyzed using the maximum likelihood method with two free parameters of the SFR and a set of the best-fit values for those parameters is obtained; they are concerned with the supernova rate as

$$R_{\text{SN}}(z) = \begin{cases} R_{\text{SN}}^0(1+z)^\alpha & \text{for } z < 1, \\ 2^\alpha R_{\text{SN}}^0 & \text{for } z > 1, \end{cases} \quad (9)$$

where R_{SN}^0 represents the local supernova rate and α determines the slope of supernova rate evolution. Although the constant SFR at $z > 1$ is assumed, it is found that the result would be the same even if this assumption is changed. This is because the bulk of the detected event comes from local supernova as already shown. (3) 10^3 such MC simulations are performed and 10^3 independent sets of best-fit parameters are obtained. Then we discuss the standard deviation of the distributions of such best-fit parameter sets and the implications for the cosmic SFR.

First we discuss the performance of Gd-SK for 5 years, or an effective volume of $22.5 \text{ kton} \cdot 5 \text{ yr}$. Because the expected event number is only ~ 10 , the parameters R_{SN}^0 and α cannot both be well determined at once. Therefore, one of those parameters should be fixed in advance at some value inferred from other observations. First, the value of R_{SN}^0 was fixed to be $1.2 \times 10^{-4} \text{ yr}^{-1} \text{ Mpc}^{-1}$, which was inferred from the local supernova survey [56], and the distribution of the best-fit values of parameter α was obtained. The result of 10^3 MC simulations are shown in figure 6(a) as a histogram of the distribution of best-fit parameters α (*solid histogram*). The average value of these 10^3 values for α is found to be 2.7, and the standard deviation is 0.8, i.e., $\alpha = 2.7 \pm 0.8$. Then in turn, the value of α was fixed to be 2.9 in order to obtain the distribution of best-fit values for the local supernova rate R_{SN}^0 from the SRN observation. The result of 10^3 MC generations and analyses in this case is shown in figure 6(b). The average value for R_{SN}^0 is $1.2 \times 10^{-4} \text{ yr}^{-1} \text{ Mpc}^{-3}$, and the standard deviation is $0.4 \times 10^{-4} \text{ yr}^{-1} \text{ Mpc}^{-3}$, i.e., $R_{\text{SN}}^0 = (1.2 \pm 0.4) \times 10^{-4} \text{ yr}^{-1} \text{ Mpc}^{-3}$. Figure 7 shows the comparison between the supernova rate model, in which the parameter is inferred from the MC simulations, and the “true” reference model; the cases of fixed R_{SN}^0 and α are shown in figures 7(a) and 7(b), respectively. The allowed region at the 1σ level is located between the two dotted curves, while the solid curve represents the reference model, from which MC data were

generated. Thus, with the Gd-SK detector we can roughly reproduce the supernova rate profile at $z < 1$ for 5 years operation.

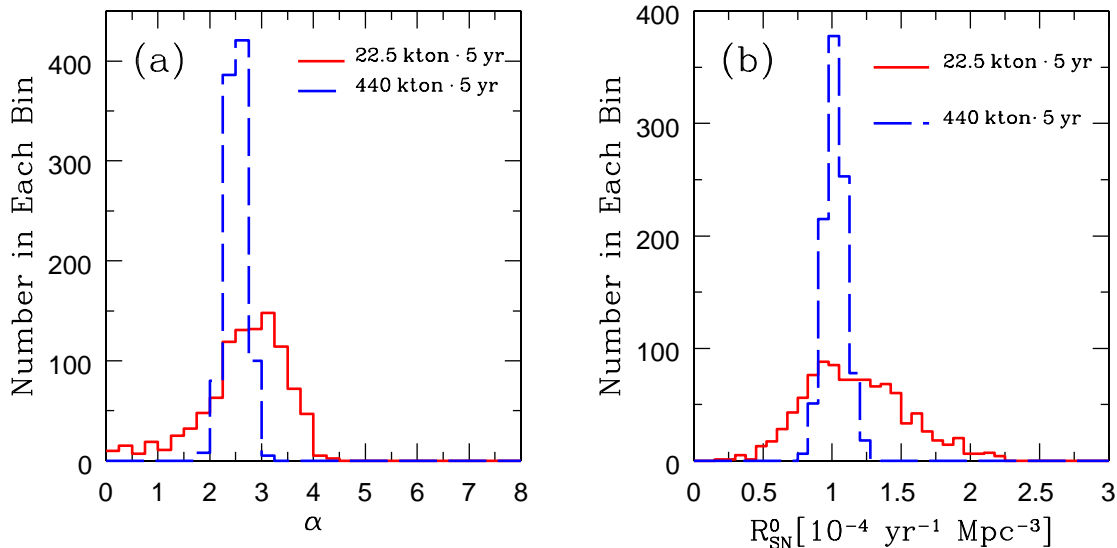


Figure 6. Distribution of 10^3 best-fit values for (a) α and (b) R_{SN}^0 , which are obtained from the analyses of each MC generation. The effective volume is $22.5 \text{ kton} \cdot 5 \text{ yr}$ for solid histogram and $440 \text{ kton} \cdot 5 \text{ yr}$ for dashed histogram. (a) The value of the local supernova rate is fixed to be $R_{\text{SN}}^0 = 1.2 \times 10^{-4} \text{ yr}^{-1} \text{ Mpc}^{-3}$. The resulting distributions are characterized by $\alpha = 2.7 \pm 0.8$ for an effective volume of $22.5 \text{ kton} \cdot 5 \text{ yr}$ and $\alpha = 2.5 \pm 0.2$ for $440 \text{ kton} \cdot 5 \text{ yr}$. (b) The value of α is fixed to be 2.9. The resulting distributions are characterized by $R_{\text{SN}}^0 = (1.2 \pm 0.4) \times 10^{-4} \text{ yr}^{-1} \text{ Mpc}^{-3}$ for $22.5 \text{ kton} \cdot 5 \text{ yr}$ and $R_{\text{SN}}^0 = (1.0 \pm 0.1) \times 10^{-4} \text{ yr}^{-1} \text{ Mpc}^{-3}$ for $440 \text{ kton} \cdot 5 \text{ yr}$. These figures are taken from [17].

Now we turn our attention to future mega-ton class detectors such as Gd-HK or Gd-UNO. With these detectors, the effective volume considered, $440 \text{ kton} \cdot 5 \text{ yr}$, is expected to be realized in several years from the start of their operation. First the same analysis as illustrated above was performed; i.e., one of relevant parameters, α or R_{SN}^0 , was fixed and the dependence on the remaining parameter was investigated. The result of these cases are also shown in figures 6(a) and 6(b) as dashed histograms, which give $\alpha = 2.5 \pm 0.2$ and $R_{\text{SN}}^0 = (1.0 \pm 0.1) \times 10^{-4} \text{ yr}^{-1} \text{ Mpc}^{-3}$, respectively. The statistical errors are considerably reduced compared with the case of $22.5 \text{ kton} \cdot 5 \text{ yr}$, because of the ~ 20 times larger effective volume. Thus, future mega-ton detectors will possibly pin down, within 10% statistical error, either the index of supernova rate evolution α or the local supernova rate R_{SN}^0 if the other is known in advance. The dashed curves in figure 7 set the allowed region of the supernova rate at the 1σ level by the considered detectors, well reproducing the assumed model. In principle, we can determine both parameters by SRN observation, because R_{SN}^0 is concerned with the absolute value of the flux alone but α is concerned with both the absolute value and the spectral shape; i.e., these two parameters are not degenerate with each other. Thus, the

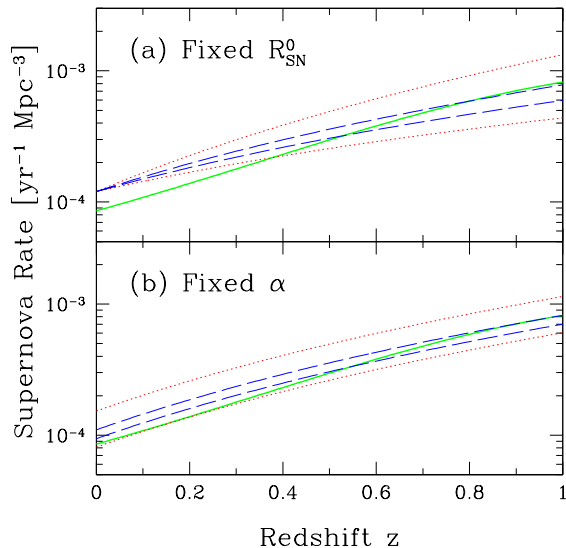


Figure 7. Supernova rate as a function of redshift. In both panels, solid curves represent the reference model, from which MC data were generated. (a) The allowed region at the 1σ level, concerning the fitting parameter α with fixed R_{SN}^0 , is shown as the area between the two dotted curves for an effective volume of $22.5 \text{ kton} \cdot 5 \text{ yr}$ and as the area between the two dashed curves for an effective volume of $440 \text{ kton} \cdot 5 \text{ yr}$. (b) The same as (a) but for fitting parameter R_{SN}^0 with fixed α . This figure is taken from [17].

same procedure was repeated but without fixing the values of α or R_{SN}^0 . The distribution of 10^3 best-fit parameter sets of $(\alpha, R_{\text{SN}}^0)$ was calculated assuming a detector with an effective volume of $440 \text{ kton} \cdot 5 \text{ yr}$; the mean values and the standard deviations were found to be $\alpha = 3.5 \pm 1.3$ and $R_{\text{SN}}^0 = (8.8 \pm 4.8) \times 10^{-5} \text{ yr}^{-1} \text{ Mpc}^{-3}$. Even though the effective volume is as large as $440 \text{ kton} \cdot 5 \text{ yr}$, it is still insufficient for determining both parameters at once.

Throughout the above arguments or those in [17], the reference SFR model with $f_* = 1$ was assumed and they seem to be dependent on the adopted values of f_* . However, the results can easily be applied to the case with other values of f_* . This is because the statistical errors are inversely proportional to the square root of the event number, which is simply proportional to $f_* V_{\text{eff}}$ in our arguments; i.e., $\delta\alpha/\langle\alpha\rangle, \delta R_{\text{SN}}^0/\langle R_{\text{SN}}^0\rangle \propto (f_* V_{\text{eff}})^{-1/2}$. In consequence, we find that the discussions given above and in [17] are quite general and can be easily modified in the other cases of f_* using the following relations:

$$\frac{\delta\alpha}{\langle\alpha\rangle} \simeq 0.3 \left(\frac{f_* V_{\text{eff}}}{22.5 \text{ kton} \cdot 5 \text{ yr}} \right)^{-1/2}, \quad \frac{\delta R_{\text{SN}}^0}{\langle R_{\text{SN}}^0\rangle} \simeq 0.3 \left(\frac{f_* V_{\text{eff}}}{22.5 \text{ kton} \cdot 5 \text{ yr}} \right)^{-1/2}. \quad (10)$$

As a next step, it would be useful to investigate the possibility that how far (to which z) we can probe the cosmic SFR by the SRN observations. As we have already shown, the main contribution to the SRN even rate at 10–30 MeV comes from low-

redshift region $0 < z < 1$. Signals from further high-redshift universe would become enhanced if we could reduce the lower energy threshold E_{th} of the SRN detection range. The value of E_{th} is restricted to 10 MeV because at energy regions lower than this, there is a large background of reactor neutrinos; its removal is impossible with the current detection methods. Since the SK and HK detectors are (will be) located at Kamioka in Japan, they are seriously affected by background neutrinos from many nuclear reactors. If some large-volume detectors were built at a location free from such background, the lower threshold energy could be reduced, enabling us to probe the high-redshift supernova rate. Ando [17] also discussed performance of future mega-ton class detectors as a function of the value of E_{th} and found that the behaviour of SFR at $1 < z < 2$ more and more affects the detected event number at $E_{\text{th}} < E_e < 30$ MeV, as we reduce the threshold energy.

6. Implication for neutrino properties

6.1. Inverted mass hierarchy

Throughout the above discussions, we have assumed normal hierarchy of neutrino masses ($m_1 \ll m_3$). However, the case of inverted mass hierarchy has not been experimentally excluded yet, and we explore this possibility in this subsection following the discussion given by Ando and Sato [14]. In this case, flavour conversions inside the supernova envelope change dramatically, compared with the normal mass hierarchy already discussed in section 2.4. Since $\bar{\nu}_3$ is the lightest, $\bar{\nu}_e$ are created as $\bar{\nu}_3$, owing to large matter potential. In that case, it is well known that at a so-called resonance point, there occurs a level crossing between $\bar{\nu}_1$ and $\bar{\nu}_3$ (for a more detailed discussion, see, e.g., [81]). At this resonance point, complete $\bar{\nu}_1 \leftrightarrow \bar{\nu}_3$ conversion occurs when the so-called adiabaticity parameter is sufficiently small compared to unity (it is said that resonance is “non-adiabatic”), while conversion never occurs when it is large (adiabatic resonance). The adiabaticity parameter γ is quite sensitive to the value of θ_{13} , i.e., $\gamma \propto \sin^2 2\theta_{13}$; when $\sin^2 2\theta_{13} \gtrsim 10^{-3}$ ($\sin^2 2\theta_{13} \lesssim 10^{-5}$), the resonance is known to be completely adiabatic (non-adiabatic) [81]. When the resonance is completely non-adiabatic (because of small θ_{13}), the situation is the same as in the case of normal mass hierarchy already discussed in section 2.4 (because $\bar{\nu}_e$ at production become $\bar{\nu}_1$ at the stellar surface), and the $\bar{\nu}_e$ spectrum after oscillation is represented by equation (7). On the other hand, adiabatic resonance (due to large θ_{13}) forces $\bar{\nu}_e$ at production to become $\bar{\nu}_3$ when they escape from the stellar surface, and therefore the observed $\bar{\nu}_e$ spectrum is given by

$$\frac{dN_{\bar{\nu}_e}}{dE_{\bar{\nu}_e}} = |U_{e3}|^2 \frac{dN_{\bar{\nu}_e}^0}{dE_{\bar{\nu}_e}} + (1 - |U_{e3}|^2) \frac{dN_{\nu_x}^0}{dE_{\nu_x}} \simeq \frac{dN_{\nu_x}^0}{dE_{\nu_x}}. \quad (11)$$

The second equality follows from the fact that the value of $|U_{e3}|^2$ is constrained to be much smaller than unity from reactor experiments [64]. Thus, equation (11) indicates that complete conversion takes place between $\bar{\nu}_e$ and ν_x . When the value of θ_{13} is large

Table 5. Flux of supernova relic neutrinos in the case of inverted mass hierarchy. Values given in this table are applicable only when the value of θ_{13} is large enough to induce completely adiabatic resonance, i.e., $\sin^2 2\theta_{13} \gtrsim 10^{-3}$. If $\sin^2 2\theta_{13} \lesssim 10^{-5}$, on the other hand, the results become the same as those given in table 2.

Model	Flux ($f_* \text{ cm}^{-2} \text{ s}^{-1}$)		
	Total	$E_\nu > 11.3 \text{ MeV}$	$E_\nu > 19.3 \text{ MeV}$
LL	9.4	3.1	0.94
TBP	13.8	1.9	0.30
KRJ	12.7	2.2	0.38

Table 6. Event rate of supernova relic neutrinos in the case of inverted mass hierarchy. Values given in this table are applicable only when the value of θ_{13} is large enough to induce completely adiabatic resonance, i.e., $\sin^2 2\theta_{13} \gtrsim 10^{-3}$. If $\sin^2 2\theta_{13} \lesssim 10^{-5}$, on the other hand, the results become the same as those in table 3.

Model	Event rate [$f_* (22.5 \text{ kton yr})^{-1}$]	
	$E_e > 10 \text{ MeV}$	$E_e > 18 \text{ MeV}$
LL	3.8	2.3
TBP	1.6	0.58
KRJ	2.0	0.76

enough to induce adiabatic resonance ($\sin^2 2\theta_{13} \gtrsim 10^{-3}$), the obtained SRN flux and spectrum should be very different from ones obtained in sections 3.1 and 3.2. The SRN flux and event rate in this case were calculated with equations (3) and (11), and the results are summarized in tables 5 and 6. The values (with the LL model) shown in this table are consistent with the calculation by [14], in which numerically calculated conversion probabilities were adopted with some specific oscillation parameter sets (which include a model with inverted mass hierarchy and $\sin^2 2\theta_{13} = 0.04$), as well as realistic stellar density profiles; they also included the shock wave propagation and the Earth matter effect in their calculations, but both were found to affect only by a few percent and irrelevant.

The total flux becomes 9.4–14 $f_* \text{ cm}^{-2} \text{ s}^{-1}$, somewhat smaller than the values given in table 2, because the total flux is dominated by the low-energy region. The fluxes at $E_\nu > 19.3 \text{ MeV}$ are enhanced to be 0.30–0.94 $f_* \text{ cm}^{-2} \text{ s}^{-1}$, but this is still below the current 90% CL upper limit of $1.2 \text{ cm}^{-2} \text{ s}^{-1}$ obtained by the SK observation if $f_* = 1$ is adopted. The event rate at the future detectable energy range, $E_\nu > 10 \text{ MeV}$, is expected to become 1.6–3.8 $f_*(22.5 \text{ kton yr})^{-1}$, which is considerably larger than the values in the case of normal mass hierarchy, 0.97–2.3 $f_*(22.5 \text{ kton yr})^{-1}$. The increase (decrease) of the flux and event rate integrated over the high (total) energy region is due to the very high efficiency of the flavour conversion, $\nu_x \rightarrow \bar{\nu}_e$, inside the supernova envelope; because the original ν_x are expected to be produced with larger

average energy as shown in table 1, the efficient conversion makes the SRN spectrum harder, which enhances the flux and event rate at the high-energy region. Thus, if the inverted mass hierarchy, as well as the large value for θ_{13} , were realized in nature, SRN detection would be rather easier, compared with the other cases. Although we do not repeat the MC simulations that were introduced in section 5.2, the results can be easily inferred; the statistical errors in this case would be $\sim (3.8/2.3)^{1/2} = 1.3$ times smaller than the values given in equation (10), because they are inversely proportional to the square root of the event number.

6.2. Resonant spin-flavour conversion

If neutrinos have non-zero magnetic moment as large as $10^{-12}\mu_B$, where μ_B is the Bohr magneton, it potentially changes supernova neutrino signal owing to an additional effect of the flavour conversions. Especially if neutrinos are the Majorana particles, the interaction between the Majorana magnetic moment and supernova magnetic fields induces a spin-flavour conversion (e.g., $\bar{\nu}_e \leftrightarrow \nu_{\mu,\tau}, \nu_e \leftrightarrow \bar{\nu}_{\mu,\tau}$) resonantly (see [65] and references therein). This mechanism could potentially give quite a characteristic supernova neutrino signal at detectors, and also is expected to affect the SRN spectrum significantly. However, it is still premature to estimate the SRN flux including the spin-flavour conversions for several reasons. First, the shock wave propagation can change the magnetic field structure as well as the density profile of supernova progenitors, both of which are essential in calculating flavour-conversion probabilities [82]. Because there is no reliable supernova simulation that succeeded in pushing the shock wave outside the core, we are even not at the stage to start the calculation. Furthermore, calculating how the propagating shock wave changes the magnetic field structure would be quite a difficult task. The second reason is that the spin-flavour conversion probabilities strongly depend on the metallicity of progenitor stars [83]. Because SRN is the accumulation of neutrinos from past supernova explosions, it should be quite natural that the poor metal stars give some contribution to the SRN flux. In consequence, it would be difficult to obtain some implication for the neutrino magnetic moment or supernova magnetic fields from the SRN detection at present; instead, a future galactic supernova neutrino burst might give some clues by its time profile or spectrum [65, 84].

6.3. Decaying neutrinos

Non-radiative neutrino decay, which is not satisfactorily constrained, potentially and significantly changes the SRN flux and spectrum. Most stringent lower limit on the neutrino lifetime-to-mass ratio comes from the solar neutrino observations [39]–[41] as well as the meson decay experiments [42]–[44], which is $\tau/m \gtrsim 10^{-4}$ s/eV. Since this limit is still very weak, neutrino decay could also change the detected signal from high-energy astrophysical objects [45] or the galactic supernova explosions [46]–[48], and could alter usual discussions on the early universe and structure formation [49] as well as on supernova coolings [50]–[52]. In this subsection, we discuss the potential consequence of

the neutrino decay on the SRN flux, with which we can obtain the most stringent limit on the neutrino lifetime in principle, as pointed out by Ando [15].

Since the flux estimation of SRNs including the neutrino decay is somewhat complicated, we rather follow a simple and intuitive argument given in [15]; exact formulation was recently derived by Fogli *et al* [18]. Ando [15] assumed the following conditions: (i) daughter neutrinos are active species; (ii) neutrino mass spectrum is quasi-degenerate ($m_1 \approx m_2 \approx m_3$); and neutrino mass hierarchy is normal. This is because the SRN flux would be most strongly enhanced owing to the decay and it might give a larger flux than the current observational limit by SK [20]; in that case the flux limit can be translated into the limit on the neutrino lifetime. He also restricted his discussion only to the helicity-conserving mode of $\bar{\nu}_3 \rightarrow \bar{\nu}_1$ and $\bar{\nu}_2 \rightarrow \bar{\nu}_1$ for simplicity, characterized by lifetimes τ_3 and τ_2 of each mode; in models discussed in [85]–[87], the above condition (ii) strongly suppresses the helicity-flip mode. In the actual calculation, instead of these lifetimes, he introduced the “decay redshift” z_i^d ($i = 2, 3$) of the mass eigenstate $\bar{\nu}_i$ as two free parameters. If the source redshift z is larger than the decay redshift z_i^d , all the neutrinos $\bar{\nu}_i$ were assumed to decay, on the other hand if $z < z_i^d$, completely survive. The relation between z_i^d and τ_i/m can be written as

$$\tau_i = \frac{mc^2}{E_\nu} \int_{z_i^d}^0 \frac{dt}{dz} dz = \frac{mc^2}{E_\nu H_0} \int_0^{z_i^d} \frac{dz}{(1+z)\sqrt{\Omega_m(1+z)^3 + \Omega_\Lambda}}, \quad (12)$$

where we assume $E_\nu = 10$ MeV as a typical neutrino energy when evaluating the lifetime τ_i from z_i^d .

Figure 8 shows the SRN flux for various parameter sets of decay redshifts (z_2^d, z_3^d) as a function of neutrino energy; the LL model as the original neutrino spectrum and $f_* = 1$ were assumed. The solid curve in figure 8 shows the SRN flux in the case that $z_2^d = z_3^d = z_{\max}(= 5)$, which represents the same flux as that without the neutrino decay. Then, the decay of the heaviest mass eigenstate $\bar{\nu}_3$ was included by his reducing the value of z_3^d , with keeping $\bar{\nu}_2$ stable. When $z_3^d = 1.0$ (dotted curve), the SRN flux at low energy region ($E_\nu \lesssim 35$ MeV) deviates from the no-decay model. This is because the neutrinos from supernovae at redshift larger than $z_3^d = 1.0$ are affected by the $\bar{\nu}_3 \rightarrow \bar{\nu}_1$ decay and it results in the increase of $\bar{\nu}_e$. Since the neutrino energies are redshifted by a factor of $(1+z)^{-1}$ owing to an expansion of the universe, the decay effect can be seen at low energy alone. When the value of z_3^d is reduced to 10^{-2} , the neutrinos even from the nearby sources are influenced by the $\bar{\nu}_3 \rightarrow \bar{\nu}_1$ decay, resulting in the deviation over the entire energy range as shown by the long-dashed curve in figure 8. If the $\bar{\nu}_2 \rightarrow \bar{\nu}_1$ decay is added, it further enhances the SRN flux. In table 7, the SRN flux integrated over the energy range of $E_\nu > 19.3$ MeV is summarized, for the each decay model. In the second column the lifetime-to-mass ratio is indicated, which corresponds to each decay redshift, which is obtained using equation (12). The ratio between the predicted flux and the 90% CL upper limit given by the SK observation [20] is also shown in the fourth column. This result shows that several decaying models may have already been excluded or severely constrained by the current SRN limit by SK. It also

Table 7. Predicted SRN flux for various decay models. The LL model is assumed as the original neutrino spectrum and integrated energy range is $E_\nu > 19.3$ MeV. The ratio of the prediction and the limit is shown in the fourth column.

Model (z_2^d, z_3^d)	$(\tau_2/m, \tau_3/m)$ (s/eV)	Predicted flux ($f_* \text{ cm}^{-2} \text{ s}^{-1}$)	Prediction/limit
(5.0, 5.0)	$(3.9 \times 10^{10}, 3.9 \times 10^{10})$	0.43	$0.35 f_*$
(5.0, 1.0)	$(3.9 \times 10^{10}, 2.4 \times 10^{10})$	0.55	$0.42 f_*$
(5.0, 0.2)	$(3.9 \times 10^{10}, 7.7 \times 10^9)$	0.93	$0.75 f_*$
(5.0, 10^{-2})	$(3.9 \times 10^{10}, 4.4 \times 10^8)$	1.0	$0.88 f_*$
($10^{-2}, 10^{-2}$)	$(4.4 \times 10^8, 4.4 \times 10^8)$	1.4	$1.2 f_*$

proves that the SRN observation can potentially give us the lower limit on the neutrino lifetime as strong as $\sim 10^{10}$ s/eV, which is many orders of magnitude stronger than that by the solar neutrino observations. In addition, future detectors such as the HK and UNO (maybe loaded with Gd) is expected to greatly improve our knowledge of the SRN spectral shape as well as its flux; if a number of data were actually acquired by such detectors, the most general and model-independent discussions concerning the neutrino decay would become accessible.

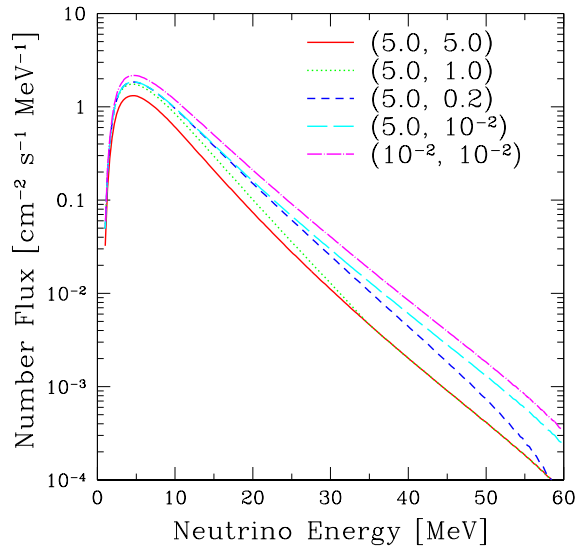


Figure 8. SRN flux for various parameter sets of decay redshifts, calculated with the LL model and $f_* = 1$. Each label represents (z_2^d, z_3^d) . This figure is taken from [15].

7. Conclusions

As stressed several times in this paper, we are at an exciting era of the SRN observation. This is because the current SK upper limit [20] is *just above* several theoretical predictions using realistic models for the cosmic SFR and supernova neutrino

spectrum, and also because of the promising technique proposed in [21] could greatly improve performance of the presently working or planned future detectors, especially for detecting SRNs. Being at such a situation, we believe that it is timely to review recent progress of theoretical and observational researches concerning SRNs from various points of view. Many physical and astronomical consequences can be derived from the constraints on the SRNs as we have reviewed through this paper.

Basics of SRN calculation were given in sections 2 and 3. Models involved in the SRN calculations are those of the cosmic SFR and original supernova neutrino spectrum. Although the SFR- z relation has been intensively studied in recent years, there remains a fair amount of uncertainty; in fact, the best estimate of the local SFR density ranges fairly widely as $(0.5\text{--}2.9)\times 10^{-2} h_{70} \text{ yr}^{-1} \text{ Mpc}^{-3}$ [54]. In order to take this uncertainty into account, we have introduced the correction factor f_* in equation (4), for which a wide range (0.7–4.2) is still allowed from the SFR observation. As for the original supernova spectrum, contrary to the traditional approach using the Fermi-Dirac distribution, we followed the approach taken by our group [12, 17], i.e., adopting the results of numerical simulations. Especially following [17], we used three neutrino spectra by different groups, i.e., LL [57], TBP [58] and KRJ [59], and performed comparison among models. Recent progress of neutrino experiments has proven that neutrinos are massive and mix among different flavours. This effect was also taken into account appropriately. As the result, it was found that the uncertainty concerning the original neutrino spectrum gives difference in the resulting SRN flux by at least a factor of 2–4. The expected event rate at a water Čerenkov detector with a fiducial volume of 22.5 kton was found to be $0.25\text{--}1 f_* \text{ yr}^{-1}$ (for $E_e > 19.3 \text{ MeV}$) and $1\text{--}2 f_* \text{ yr}^{-1}$ (for $E_e > 10 \text{ MeV}$), depending on these supernova models (see table 3).

Besides the flux estimation, a careful discussion about background events is definitely necessary in order to investigate the detectability. This has been thoroughly argued in [12] and we followed them in section 4. The most serious background comes from decay products of invisible muons, which are produced almost at rest inside the detector and that is why “invisible.” Because of the background, the detection is severely restricted; for a pure-water Čerenkov detector with the size of SK, it would take about (maybe more than) 10 years in order to reach the signal-to-noise ratio of a few (see figure 5). We also discussed performance of other detectors such as SNO and KamLAND in the same section, by mainly following [12, 16]. The current observational upper limit by SK [20] and the proposed technique that potentially improves the performance of water Čerenkov detectors [21] were briefly introduced there. In addition, we showed that the SK limit on the SRN flux can be fairly well reproduced by a simple statistical argument using equation (8).

Section 5 was devoted to the discussion on the current status and future prospects for obtaining limits on the cosmic SFR from the SRN observations. We first showed that the current SRN limit from SK [20] already sets a stringent limit on the local SFR value, as discussed in [13]. Surprisingly, it might rule out a part of local SFR value allowed by the current observations using the light as shown in table 4. Performance

of future detectors loaded with Gd as proposed in [21] was investigated in detail using the MC simulation, following discussion in [17]. The distribution of the best-fit values of two parameters concerning SFR (9) was obtained by the generated 10^3 MC data and by accompanying likelihood analyses. If one of two free parameters was fixed somehow in advance using other observations, then the SRN observation can constrain the remaining parameter by accuracy of $\sim 0.3(f_*V_{\text{eff}}/22.5 \text{ kton} \cdot 5 \text{ yr})^{-1/2}$; this number would soon become quite significant if the future mega-ton class detectors such as HK or UNO loaded with Gd started data-taking.

Finally in section 6, SRN constraints on particle physics models of neutrinos were discussed. Neutrino oscillations in the case of inverted mass hierarchy [14], resonant spin-flavour conversions induced by the neutrino magnetic moment (see [65] and references therein) and neutrino decay [15, 18] are expected to considerably change the SRN signal at the detectors. In particular for neutrino decay model, the SRN observation potentially gives the most stringent constraint on the neutrino lifetime, compared with a galactic supernova [46]–[48], high-energy astrophysical objects [45] as well as the most reliable (but weak) limit at present by the solar neutrino observations [39]–[41].

Acknowledgments

SA's work is supported by a Grant-in-Aid for JSPS Fellows. KS's work is supported in part by a Grant-in-Aid for Scientific Research provided by the Ministry of Education, Culture, Sports, Science and Technology of Japan through Research Grant No S14102004, a Grant-in-Aid for Scientific Research on priority Areas No 14079202.

References

- [1] Bisnovatyi-Kogan G S and Seidov S F 1984 *Ann. N.Y. Acad. Sci.* **422** 319
- [2] Krauss L M, Glashow S L and Schramm D N 1984 *Nature* **310** 191
- [3] Woosley S E, Wilson J R and Mayle R 1986 *Astrophys. J.* **302** 19
- [4] Hirata K S 1991 Ph.D. thesis, University of Tokyo
- [5] Totsuka Y 1992 *Rep. Prog. Phys.* **55** 377
- [6] Suzuki H 1994 *Supernova neutrinos*, in: Fukugita M and Suzuki A (eds), *Physics and Astrophysics of Neutrinos* (Tokyo: Springer-Verlag) p 764
- [7] Totani T and Sato K 1995 *Astropart. Phys.* **3** 367
- [8] Totani T, Sato K and Yoshii Y 1996 *Astrophys. J.* **460** 303
- [9] Malaney R A 1997 *Astropart. Phys.* **7** 125
- [10] Hartmann D H and Woosley S E 1997 *Astropart. Phys.* **7** 137
- [11] Kaplinghat M, Steigman G and Walker T P 2000 *Phys. Rev. D* **62** 043001
- [12] Ando S, Sato K and Totani T 2003 *Astropart. Phys.* **18** 307
- [13] Fukugita M and Kawasaki M 2003 *Mon. Not. R. Astron. Soc.* **340** L7
- [14] Ando S and Sato K 2003 *Phys. Lett. B* **559** 113
- [15] Ando S 2003 *Phys. Lett. B* **570** 11
- [16] Strigari L E, Kaplinghat M, Steigman G and Walker T P 2004 *J. Cosmol. Astropart. Phys.* JCAP03(2004)007
- [17] Ando S 2004 *Astrophys. J.* **607** 20
- [18] Fogli G L, Lisi E, Mirizzi A and Montanino D 2004 *Phys. Rev. D* **70** 013001

- [19] Cocco A G, Ereditato A, Fiorillo G, Mangano G and Pettorino V 2004 *Preprint* hep-ph/0408031
- [20] Malek M *et al* 2003 *Phys. Rev. Lett.* **90** 061101
- [21] Beacom J F and Vagins M R 2003 *Preprint* hep-ph/0309300
- [22] Lilly S, Fèvre O L, Hammer F and Crampton D 1996 *Astrophys. J.* **460** L1
- [23] Madau P, Ferguson H C, Dickinson M E, Giavalisco M, Steidel C C and Fruchter A 1996 *Mon. Not. R. Astron. Soc.* **283** 1388
- [24] Cowie L, Songaila A, Hu E and Cohen J 1996 *Astron. J.* **112** 839
- [25] Connolly A, Szalay A, Dickinson M, Rao M S and Brunner R 1997 *Astrophys. J.* **486** L11
- [26] Sawicki M J, Lin H and Yee H K C 1997 *Astron. J.* **113** 1
- [27] Treyer M, Ellis R, Milliard B, Donas J and Bridges T 1998 *Mon. Not. R. Astron. Soc.* **300** 303
- [28] Madau P, Pozzetti L and Dickinson M 1998 *Astrophys. J.* **498** 106
- [29] Pascarelle S M, Lanzetta K M and Fernandez-Soto A 1998 *Astrophys. J.* **508** L1
- [30] Steidel C C, Adelberger K L, Giavalisco M, Dickinson M and Pettini M 1999 *Astrophys. J.* **519** 1
- [31] Hughes D H *et al* 1998 *Nature* **394** 241
- [32] Flores H *et al* 1999 *Astrophys. J.* **517** 148
- [33] Gallego J, Zamorano J, Aragón-Salamanca A and Rego M 1995 *Astrophys. J.* **455** L1
- [34] Gronwall C 1998 in: Thuan T *et al* (eds), *Proc. 33rd Rencontres de Moriond, Dwarf Galaxies and Cosmology* (Gif-sur-Yvette: Editions Frontières) p 41
- [35] Tresse L and Maddox S 1998 *Astrophys. J.* **495** 691
- [36] Glazebrook K, Blake C, Economou F, Lilly S and Colless M 1999 *Mon. Not. R. Astron. Soc.* **306** 843
- [37] Somerville R S, Primack J R and Faber S M 2001 *Mon. Not. R. Astron. Soc.* **320** 504
- [38] Glazebrook K *et al* 2003 *Astrophys. J.* **587** 55
- [39] Beacom J F and Bell N F 2002 *Phys. Rev. D* **65** 113009
- [40] Bandyopadhyay A, Choubey S and Goswami S 2003 *Phys. Lett. B* **555** 33
- [41] Eguchi K *et al* 2003 *Phys. Rev. Lett.* **92** 071301
- [42] Barger V D, Keung W Y and Pakvasa S 1982 *Phys. Rev. D* **25** 907
- [43] Picciotto C E *et al* 1988 *Phys. Rev. D* **37** 1131
- [44] Britton D I *et al* 1994 *Phys. Rev. D* **49** 28
- [45] Beacom J F, Bell N F, Hooper D, Pakvasa S and Weiler T J 2003 *Phys. Rev. Lett.* **90** 181301
- [46] Frieman J A, Haber H E and Freese K 1988 *Phys. Lett. B* **200** 115
- [47] Raghavan R S, He X G and Pakvasa S 1988 *Phys. Rev. D* **38** 1317
- [48] Ando S 2004 *Phys. Rev. D* **70** 033004
- [49] Beacom J F, Bell N F and Dodelson S 2004 *Phys. Rev. Lett.* **93** 121302
- [50] Fuller G M, Mayle R and Wilson J R 1988 *Astrophys. J.* **332** 826
- [51] Kachelriess M, Tomàs R and Valle J W F 2000 *Phys. Rev. D* **62** 023004
- [52] Farzan Y 2003 *Phys. Rev. D* **67** 073015
- [53] Porciani C and Madau P 2001 *Astrophys. J.* **548** 522
- [54] Baldry I K and Glazebrook K 2003 *Astrophys. J.* **593** 258
- [55] Scalo J 1998 *The IMF Revisited: A Case for Variations*, in: ASP Conf. Ser. 142: *The Stellar Initial Mass Function (38th Herstmonceux Conf.)* p 201
- [56] Madau P, della Valle M and Panagia N 1998 *Mon. Not. R. Astron. Soc.* **297** 17
- [57] Totani T, Sato K, Dalhed H E and Wilson J R 1998 *Astrophys. J.* **496** 216
- [58] Thompson T A, Burrows A and Pinto P 2003 *Astrophys. J.* **592** 434
- [59] Keil M T, Raffelt G G and Janka H T 2003 *Astrophys. J.* **590** 971
- [60] Fukuda S *et al* 2002 *Phys. Lett. B* **539** 179
- [61] Ahmed S N *et al* 2004 *Phys. Rev. Lett.* **92** 181301
- [62] Fukuda Y *et al* 1999 *Phys. Rev. Lett.* **82** 2644
- [63] Eguchi K *et al* 2003 *Phys. Rev. Lett.* **90** 021802
- [64] Apollonio M *et al* 1999 *Phys. Lett. B* **466** 415
- [65] Ando S and Sato K 2003 *J. Cosmol. Astropart. Phys.* JCAP10(2003)001

- [66] Gaisser T K, Stanev T and Barr G 1988 *Phys. Rev. D* **38** 85
- [67] Barr G, Gaisser T K and Stanev T 1989 *Phys. Rev. D* **39** 3532
- [68] Vogel P and Beacom J F 1999 *Phys. Rev. D* **60** 053003
- [69] Strumia A and Vissani F 2003 *Phys. Lett. B* **564** 42
- [70] Kajita T and Totsuka Y 2001 *Rev. Mod. Phys.* **73** 85
- [71] Battistoni G, Ferrari A, Lipari P, Montaruli T, Sala P R and Rancati T 2000 *Astropart. Phys.* **12** 315
- [72] Lipari P, Stanev T and Gaisser T K 1998 *Phys. Rev. D* **58** 073003
- [73] Agrawal V, Gaisser T K, Lipari P and Stanev T 1996 *Phys. Rev. D* **53** 1314
- [74] Honda M, Kajita T, Kasahara K and Midorikawa S 1995 *Phys. Rev. D* **52** 4985
- [75] Bahcall J N 1989 *Neutrino Astrophysics* (Cambridge University Press)
- [76] Bemporad C, Gratta G and Vogel P 2002 *Rev. Mod. Phys.* **74** 297
- [77] Schreckenbach K *et al* 1985 *Phys. Lett. B* **160** 325
- [78] Hahn A A *et al* 1989 *Phys. Lett. B* **218** 365
- [79] Vogel P and Engel J 1989 *Phys. Rev. D* **39** 3378
- [80] Hargrove C K, Blevis I, Paterson D and Earle E D 1995 *Nucl. Instrum. Methods A* **357** 157
- [81] Dighe A S and Smirnov A Yu 2000 *Phys. Rev. D* **62** 033007
- [82] Ando S and Sato K 2003 *Phys. Rev. D* **67** 023004
- [83] Ando S and Sato K 2003 *Phys. Rev. D* **68** 023003
- [84] Akhmedov E Kh and Fukuyama T 2003 *J. Cosmol. Astropart. Phys.* JCAP12(2003)007
- [85] Kim C W and Lam W P 1990 *Mod. Phys. Lett. A* **5** 297
- [86] Berezhiani Z G, Fiorentini G, Moretti M and Rossi A 1992 *Z. Phys. C* **54** 581
- [87] Giunti C, Kim C W, Lee U W and Lam W P 1992 *Phys. Rev. D* **45** 1557